

PAPER • OPEN ACCESS

## Evolution of Power Anisotropy in Magnetic Field Fluctuations at Different Solar Activity Levels

To cite this article: L Adhikari *et al* 2018 *J. Phys.: Conf. Ser.* **1100** 012001

View the [article online](#) for updates and enhancements.



**IOP | ebooks™**

Bringing you innovative digital publishing with leading voices to create your essential collection of books in STEM research.

Start exploring the collection - download the first chapter of every title for free.

# Evolution of Power Anisotropy in Magnetic Field Fluctuations at Different Solar Activity Levels

L Adhikari<sup>1</sup>, G P Zank<sup>1,2</sup>, L L Zhao<sup>1</sup>, D Telloni<sup>3</sup>, P Hunana<sup>1,2</sup>,  
and D Shiota<sup>4,5</sup>

<sup>1</sup>Center for Space Plasma and Aeronomic Research (CSPAR), University of Alabama in Huntsville, Huntsville, AL 35899, USA

<sup>2</sup>Department of Space Science, University of Alabama in Huntsville, Huntsville, AL 35899, USA

<sup>3</sup>INAF - Astrophysical Observatory of Torino, Via Osservatorio 20, 10025 Pino Torinese, Italy

<sup>4</sup>Institute for Space-Earth Environmental Research, Nagoya University, Nagoya, Aichi 464-8601, Japan

<sup>5</sup>National Institute of Information and Communications Technology (NICT), Koganei, Tokyo, 184-8795, Japan

E-mail: [1a0004@uah.edu](mailto:1a0004@uah.edu)

**Abstract.** Adhikari et al [33] recently developed a theoretical model to study anisotropy in magnetic field fluctuations using a dimensional analysis relating the power spectrum of the energy-containing and inertial ranges. We use the Adhikari et al and Zank et al [31] models to study the evolution of the power anisotropy in magnetic field fluctuations in the energy-containing and inertial ranges at different levels of solar activity. We obtain initial conditions at 1 au for the times 2003, 2009, and 2015 from Zhao et al [37] by assuming an 80:20 ratio between the turbulence energies, and a 2:1 ratio between the correlation lengths. The years 2003 and 2015 correspond to solar maxima and the year 2009 to a solar minimum. We find that the anisotropy in magnetic field fluctuations evolves differently during the solar minimum than during the solar maximum throughout the heliosphere.

## 1. Introduction

Anisotropy, an intrinsic property of the solar wind, arises due to a presence of a large-scale magnetic field  $\mathbf{B}_0$  [1 - 3]. Anisotropy in the presence of  $\mathbf{B}_0$  is indicated by unequal variances in the velocity and magnetic field fluctuations along the direction parallel and perpendicular to  $\mathbf{B}_0$ . Anisotropy is an important local property of the solar wind turbulence. Understanding the anisotropy of solar wind fluctuations may assist us in understanding solar wind turbulence and the propagation and acceleration of cosmic



rays [4 - 6]. Several theoretical and numerical methods [7 - 12] have been utilized to study anisotropy in a magnetized plasma such as the solar wind or a laboratory plasma. Some studies [13 - 18] investigate the anisotropy by calculating the energy spectrum of magnetohydrodynamic (MHD) turbulence. Others consider the variance of magnetic field fluctuations in directions parallel and perpendicular to the large-scale magnetic field [19 - 21].

The availability of single- and multi-spacecraft measurements has significantly increased our understanding of anisotropy in solar wind fluctuations [22 - 27]. The anisotropy of solar wind fluctuations in the fast and slow solar wind [28], and solar maximum and solar minimum [29] is found to be different. Moreover, the anisotropy may also depend on helio-latitude. Fluctuations in the fast wind tend to be more isotropic, while fluctuations in the slow wind are more anisotropic. Zank and Matthaeus [30] (and other studies [4, 28]) suggested that the solar wind at 1 au contains a majority of 2D fluctuations with a minority slab component. These studies put forward an 80:20 ratio between the 2D and slab turbulence, but this ratio can vary due to the dependency of anisotropy on the fast and slow solar wind, solar maximum and minimum, and higher and lower latitude.

Zank et al [31] (see also [32, 33, 34]) developed 2D and slab turbulence transport equations using a nearly incompressible (NI) phenomenology based on the inhomogeneous MHD model of Hunana and Zank [35]. Zank et al [31], and Adhikari et al [33] investigated the 2D and slab turbulence intensities using an 80:20 energy ratio between the 2D and slab turbulence at 1 au. Later, Adhikari et al [34] solved the 2D and slab NI turbulence transport equations throughout the heliosphere using 80:20, 70:30, 60:40, and 55:45 initial energy ratios between the 2D and slab turbulence at 1 au. Adhikari et al [34] found that the turbulence energies change a little, and the trends are similar. Adhikari et al [36] using the NI turbulence model of Zank et al [31] presented the evolution of anisotropy in magnetic field fluctuations in the energy-containing and inertial ranges throughout the heliosphere. Adhikari et al [36] found that an anisotropy in magnetic field fluctuations exists within  $\sim 20$  au, but the fluctuations in the outer heliosphere revert to an almost isotropic state. In this paper, we study the anisotropy in magnetic field fluctuations for different solar activity levels using the boundary conditions that Zhao et al [37] derived observationally. Table 2 of Zhao et al shows the values of the turbulence quantities at 1 au for the years 2003, 2009, and 2015. We note that the years 2003 and 2015 correspond to solar maxima and year 2009 to solar minimum. The 2003 solar maximum is stronger than the 2015 solar maximum. We present a theoretical model in Section 2, and discuss our results in Section 3. Finally, we summarize our results and present conclusions in Section 4.

## 2. Theory

In this section, we present a theoretical model for the anisotropy in magnetic field fluctuations in the inertial range. The details of the derivation of the model are described in Adhikari et al [36]. The variances of the 2D and slab magnetic field fluctuations are given by [36, 38]

$$\langle B_{2D}^2 \rangle = 2\pi \int g^{2D}(\mathbf{k}_\perp) d\mathbf{k}_\perp \quad \text{and} \quad \langle b_{sl}^2 \rangle = 4\pi \int g^{slab}(k_\parallel) dk_\parallel, \quad (1)$$

where  $\mathbf{k}_\perp$  and  $k_\parallel$  are the perpendicular and parallel wave vectors.  $g$  is a function of the perpendicular and parallel wave number. We assume a power spectrum  $g = Ck^{-1}$  and  $g = Dk^{-5/3}$  in the energy-containing and inertial range, respectively, and  $C$  and  $D$  are constants. Suppose  $g^{2D} = C^{2D}k_\perp^{-1}$  and  $g^{slab} = C^{slab}k_\parallel^{-1}$  for the 2D and slab turbulence, respectively, and then integrate Equation (1) from  $k_{inj}$  to  $k_b$  to obtain [36]

$$C_{ER}^{2D} \equiv \frac{\langle B_{2D}^2 \rangle_{ER}}{\log\left(\frac{(l_b^{2D})^{-1}}{k_{inj}}\right)} \quad \text{and} \quad C_{ER}^{slab} \equiv \frac{\langle b_{slab}^2 \rangle_{ER}}{\log\left(\frac{(l_b^{slab})^{-1}}{k_{inj}}\right)}, \quad (2)$$

where  $ER$  indicates energy-containing range,  $k_{inj}$  is a large-scale injection wave number,  $k_b$  ( $\sim l_b^{-1}$ ) is a wave number that separates the energy-containing and inertial range, and  $l_b^{2D}$  and  $l_b^{slab}$  are the correlation lengths of the variances of the 2D and slab magnetic field fluctuations. From Equation (2), we obtain the ratio between the  $C_{ER}^{2D}$  and  $C_{ER}^{slab}$  as [36],

$$\frac{C_{ER}^{2D}}{C_{ER}^{slab}} = \frac{\langle B_{2D}^2 \rangle_{ER}}{\langle b_{slab}^2 \rangle_{ER}} \frac{\log\left(\frac{(l_b^{slab})^{-1}}{k_{inj}}\right)}{\log\left(\frac{(l_b^{2D})^{-1}}{k_{inj}}\right)}. \quad (3)$$

Equation (3) describes the ratio of the 2D and slab variances of magnetic field fluctuations in the energy-containing range. Now, we calculate the ratio of the variances of the 2D and slab magnetic field fluctuations in the inertial range. Since the wave number  $k_b$  separates the energy-containing and inertial range, we can write  $Ck^{-1}|_{k_b} = Dk^{-5/3}|_{k_b}$ , which yields  $D = Ck_b^{2/3}$ . Therefore, the power spectrum for the 2D and slab turbulence in the inertial range can be written as  $g^{2D} = C_{ER}^{2D}(k_b^{2D})^{2/3}k_\perp^{-5/3}$  and  $g^{sl} = C_{ER}^{sl}(k_b^{sl})^{2/3}k_\parallel^{-5/3}$ , respectively. We use  $g^{2D}$  in Equation (1) and integrate the equation from  $k_1^{2D}$  to  $k_2^{2D}$ , so that we consider the anisotropy in a wave number range  $[k_1^{2D}, k_2^{2D}]$ . Here,  $k_1^{2D}$  and  $k_2^{2D}$  are arbitrary wave numbers, and the  $k_b^{2D} < k_1^{2D} < k_2^{2D}$  inequality is satisfied. The variance of the 2D magnetic field fluctuations is [36]

$$\begin{aligned} \langle B_{2D}^2 \rangle_{IR} &\equiv C_{ER}^{2D}(k_b^{2D})^{2/3} \int_{k_1^{2D}}^{k_2^{2D}} k_\perp^{-5/3} dk_\perp, \\ &= \frac{3}{2}C_{ER}^{2D}(k_b^{2D})^{2/3}((k_1^{2D})^{-2/3} - (k_2^{2D})^{-2/3}), \end{aligned} \quad (4)$$

where IR denotes the inertial range. Similarly, we obtain the variance of the slab magnetic field fluctuations as [36]

$$\begin{aligned} \langle b_{slab}^2 \rangle_{IR} &\equiv C_{ER}^{sl}(k_b^{slab})^{2/3} \int_{k_1^{slab}}^{k_2^{slab}} k_\parallel^{-5/3} dk_\parallel, \\ &= \frac{3}{2}C_{ER}^{slab}(k_b^{slab})^{2/3}((k_1^{slab})^{-2/3} - (k_2^{slab})^{-2/3}). \end{aligned} \quad (5)$$

Here,  $g^{slab}(k_{\parallel}) = C_{ER}^{slab}(k_b^{slab})^{2/3}k_{\parallel}^{-5/3}$  is used in Equation (1), and the integral is integrated from  $k_1^{slab}$  and  $k_2^{slab}$ , where  $k_1^{slab}$  and  $k_2^{slab}$  are arbitrary wave numbers such that  $k_b^{slab} < k_1^{slab} < k_2^{slab}$ . Now, dividing Equation (4) by Equation (5) yields

$$\frac{\langle B_{2D}^2 \rangle_{IR}}{\langle b_{slab}^2 \rangle_{IR}} = \frac{C_{ER}^{2D}}{C_{ER}^{slab}} \left( \frac{k_b^{2D}}{k_b^{slab}} \right)^{2/3} \frac{((k_1^{2D})^{-2/3} - (k_2^{2D})^{-2/3})}{((k_1^{slab})^{-2/3} - (k_2^{slab})^{-2/3})},$$

and by assuming  $k_1^{2D} = k_1^{slab}$  and  $k_2^{2D} = k_2^{slab}$ , we obtain

$$\frac{\langle B_{2D}^2 \rangle_{IR}}{\langle b_{slab}^2 \rangle_{IR}} = \frac{C_{ER}^{2D}}{C_{ER}^{slab}} \left( \frac{k_b^{2D}}{k_b^{slab}} \right)^{2/3}. \quad (6)$$

Equations (3) and (6) yield the ratio of the variances of the 2D and slab magnetic field fluctuations in the inertial range [36],

$$\frac{\langle B_{2D}^2 \rangle_{IR}}{\langle b_{slab}^2 \rangle_{IR}} = \frac{\langle B_{2D}^2 \rangle_{ER}}{\langle b_{slab}^2 \rangle_{ER}} \left( \frac{l_b^{slab}}{l_b^{2D}} \right)^{2/3} \frac{\log \left( \frac{(l_b^{slab})^{-1}}{k_{inj}} \right)}{\log \left( \frac{(l_b^{2D})^{-1}}{k_{inj}} \right)}, \quad (7)$$

We use Equation (7) to study the anisotropy of magnetic field fluctuations in the inertial range. In Equation (7), the turbulence parameters  $\langle B_{2D}^2 \rangle_{ER}$ ,  $\langle b_{slab}^2 \rangle_{ER}$ ,  $l_b^{slab}$ , and  $l_b^{2D}$  on the right hand side are associated with the energy-containing range, and are obtained from the NI turbulence transport model equations of Zank et al [31]. These large-scale turbulence quantities are calculated as [31]

$$\left\langle \frac{B^{2D,*2}}{\mu_0 \rho} \right\rangle = \frac{\langle z^{\infty,*+2} \rangle + \langle z^{\infty,*-2} \rangle - 2E_D^{\infty,*}}{4}, \quad \text{and} \quad (8)$$

$$l_b^{\infty,*} = \frac{L_+^{\infty,*} + L_-^{\infty,*} - L_D^{\infty,*}}{\langle z^{\infty,*+2} \rangle + \langle z^{\infty,*-2} \rangle - 2E_D^{\infty,*}},$$

where  $\mu_0$  is the magnetic permeability of free space and  $\rho$  is the solar wind density. In Equation (8), “ $\infty$ ” indicates 2D turbulence, and “\*” indicates slab turbulence. The parameters  $\langle z^{\pm 2} \rangle$  and  $E_D$  are the energies in forward and backward propagating modes, and the residual energy, and  $L^{\pm}$  and  $L_D$  are the corresponding correlation functions [31]. In Equation (7),  $k_{inj} \sim 1.07 \times 10^{-9} \text{ km}^{-1}$ , which corresponds to one solar rotation ( $\sim 27$  days). Moreover, the stream-shear sources of 2D turbulence for the forward and backward propagating modes, and the residual energy are [31, 33, 39]

$$S_{\langle z^{\pm 2} \rangle} = \frac{C_{sh}^{\pm} r_0 |\Delta U| V_{A0}^2}{r^2}; \quad S_{E_D} = \frac{C_{sh}^{E_D} r_0 |\Delta U| V_{A0}^2}{r^2}, \quad (9)$$

where  $r_0=1$  au,  $V_{A0}$  is the Alfvén velocity at 1 au, and  $C_{sh}^{\pm}$  and  $C_{sh}^{E_D}$  are stream-shear driving constants for the forward and backward propagating modes, and the residual

energy. Similarly, the stream-shear and pickup ion sources of slab turbulence are [31, 33, 39]

$$\begin{aligned} S_{\langle z^{\pm*2} \rangle} &= \frac{C_{sh}^{*\pm} r_0 |\Delta U| V_{A0}^2}{r^2}; & S_{E_D} &= \frac{C_{sh}^{*E_D} r_0 |\Delta U| V_{A0}^2}{r^2}, \\ S_{\text{PUI}} &= \frac{f_D n_H^\infty U V_{A0}}{n_{sw}^0 \tau_{ion}^0} \exp(-L/r), \end{aligned} \quad (10)$$

where  $L$  ( $=8$  au) is the ionization cavity length scale,  $f_D$  is the fraction of pickup ion energy transferred into excited waves, and  $C_{sh}^{*\pm}$  and  $C_{sh}^{*E_D}$  are stream-shear driving constants of the slab turbulence. The parameter  $n_H^\infty$  ( $=0.1 \text{ cm}^{-3}$ ) is the number density of interstellar neutrals entering the heliosphere,  $\tau_{ion}^0$  ( $=10^6$  s) is the neutral ionization time at 1 AU,  $n_{sw}^0$  is the solar wind density at 1 AU, and  $U$  is the solar wind speed. Strengths of the stream-shear sources of 2D and slab turbulence, and the pickup ion source of slab turbulence are shown in Table 3.

### 3. Results

In this section, we show the ratio of the variances of the 2D and slab magnetic field fluctuations  $\langle B_{2D}^2 \rangle / \langle b_{slab}^2 \rangle$  in the energy-containing and inertial ranges throughout the heliosphere from 1 to 75 au. First, we solve the NI turbulence transport equations of Zank et al [31] using the boundary conditions and solar wind parameter values shown in Tables 1 and 2, respectively, for three cases; i) no source of turbulence, ii) stream-shear sources of 2D and slab turbulence, and iii) stream-shear sources of 2D and slab turbulence, and a pickup ion source of turbulence. Table 1 shows the boundary conditions for the three years 2003, 2009, and 2015, from which we calculate the ratio  $\langle B_{2D}^2 \rangle / \langle b_{slab}^2 \rangle$  in the energy-containing and inertial ranges for these three years. The boundary conditions are obtained from Zhao et al [37], and we assume an 80:20 energy ratio between the 2D and slab turbulence, and that  $\lambda^* = 2\lambda^\infty$  for the correlation lengths, where  $\lambda^\infty$  is the 2D correlation length and  $\lambda^*$  is the slab correlation length.

The ratios of the variances of the 2D and slab magnetic field fluctuations with no source of turbulence, stream-shear sources of 2D and slab turbulence, and stream-shear sources of 2D and slab turbulence and a pickup ion source of slab turbulence are shown in Figures 1, 2, and 3, respectively. In the figures, the blue, red, and green curves correspond to the boundary conditions for the years 2003, 2009, and 2015, respectively. Furthermore, the solid curves denote the  $\langle B_{2D}^2 \rangle / \langle b_{slab}^2 \rangle$  ratio in the inertial range, and the dashed curves the  $\langle B_{2D}^2 \rangle / \langle b_{slab}^2 \rangle$  in the energy-containing range.

Figure 1 shows the evolution of anisotropy in magnetic field fluctuations in the energy-containing and inertial ranges when an interplanetary source of turbulence is not included in the turbulence transport model equations. The energy-containing range results (dashed curves) show that the  $\langle B_{2D}^2 \rangle / \langle b_{slab}^2 \rangle$  ratio during solar minimum (i.e., 2009) increases monotonically with distance. However, the  $\langle B_{2D}^2 \rangle / \langle b_{slab}^2 \rangle$  ratio corresponding to the solar maxima (i.e., 2003 and 2015) decreases slightly between  $\sim 1.2-2$  au and then increases with heliocentric distance. The results indicate that the  $\langle B_{2D}^2 \rangle / \langle b_{slab}^2 \rangle$  ratio for the 2009 solar minimum is larger than the two  $\langle B_{2D}^2 \rangle / \langle b_{slab}^2 \rangle$  ratios corresponding to the 2003 and 2015 solar maxima. Furthermore, the 2003 solar maximum  $\langle B_{2D}^2 \rangle / \langle b_{slab}^2 \rangle$  ratio

Parameters	2003	2009	2015
$\langle z^{\infty+2} \rangle$ ( $\text{km}^2\text{s}^{-2}$ )	474.98	176.81	303.32
$\langle z^{\infty-2} \rangle$ ( $\text{km}^2\text{s}^{-2}$ )	1219.34	290.46	503.85
$E_D^\infty$ ( $\text{km}^2\text{s}^{-2}$ )	-346.23	-90.89	-160.94
$L_\infty^+$ ( $\text{km}^3\text{s}^{-2}$ )	$1.93 \times 10^8$	$3.94 \times 10^7$	$9.2 \times 10^7$
$L_\infty^-$ ( $\text{km}^3\text{s}^{-2}$ )	$6.95 \times 10^8$	$9.36 \times 10^7$	$2.6 \times 10^8$
$L_D^\infty$ ( $\text{km}^3\text{s}^{-2}$ )	$-4.30 \times 10^8$	$-7.18 \times 10^7$	$-1.5 \times 10^8$
$\langle z^{*+2} \rangle$ ( $\text{km}^2\text{s}^{-2}$ )	118.75	44.2	75.83
$\langle z^{*-2} \rangle$ ( $\text{km}^2\text{s}^{-2}$ )	304.83	72.62	125.96
$E_D^*$ ( $\text{km}^2\text{s}^{-2}$ )	-86.56	-22.72	-40.23
$L_*^+$ ( $\text{km}^3\text{s}^{-2}$ )	$9.64 \times 10^7$	$1.96 \times 10^7$	$4.6 \times 10^7$
$L_*^-$ ( $\text{km}^3\text{s}^{-2}$ )	$3.48 \times 10^8$	$4.68 \times 10^7$	$1.3 \times 10^8$
$L_D^*$ ( $\text{km}^3\text{s}^{-2}$ )	$-2.15 \times 10^8$	$-3.59 \times 10^7$	$-7.5 \times 10^7$

**Table 1.** Boundary conditions for the years 2003, 2009, and 2015 at 1 au. These values are obtained from Zhao et al [37] by assuming an 80:20 energy ratio between 2D and slab turbulence, and a 2:1 ratio between the correlation lengths for slab and 2D turbulence.

Parameters	2003	2009	2015
$n$ ( $\text{cm}^{-3}$ )	5.33	6.02	6.96
$U$ ( $\text{kms}^{-1}$ )	493.31	359.48	412.25
$V_A$ ( $\text{kms}^{-1}$ )	88.10	43.21	66.86
$B$ (nT)	8.14	4.41	7.42
$\Delta UV_A^2$ ( $\text{km}^3\text{s}^{-3}$ )	$1.93 \times 10^6$	$2.29 \times 10^5$	$8.25 \times 10^5$

**Table 2.** Solar wind parameter values at 1 au (Zhao et al [37]).

Parameters	case (i)	case (ii)	case (iii)
$C_{sh}^+$	0	0.9	0.9
$C_{sh}^-$	0	0.9	0.9
$C_{sh}^{E_D}$	0	-0.5	-0.5
$C_{sh}^{*+}$	0	0.3	0.3
$C_{sh}^{*-}$	0	0.3	0.3
$C_{sh}^{*E_D}$	0	-0.17	-0.17
$f_{sh}^D$	0	0	0.25
$f_{sh}^D$	0	0	0.24

**Table 3.** Strengths of the stream-shear sources of 2D and slab turbulence, and a pickup ion source of slab turbulence (Adhikari et al [33]).

is smaller than that of the 2015 solar maximum. Note that the 2003 solar maximum is stronger than the 2015 solar maximum. The energy-containing range anisotropy is larger during solar minimum than solar maximum. The energy-containing range anisotropy is quite sizable throughout the heliosphere, being between  $\sim 4.5$  and  $\sim 5.5$  for all

solar conditions (maximum and minimum). The inertial range results exhibit similar

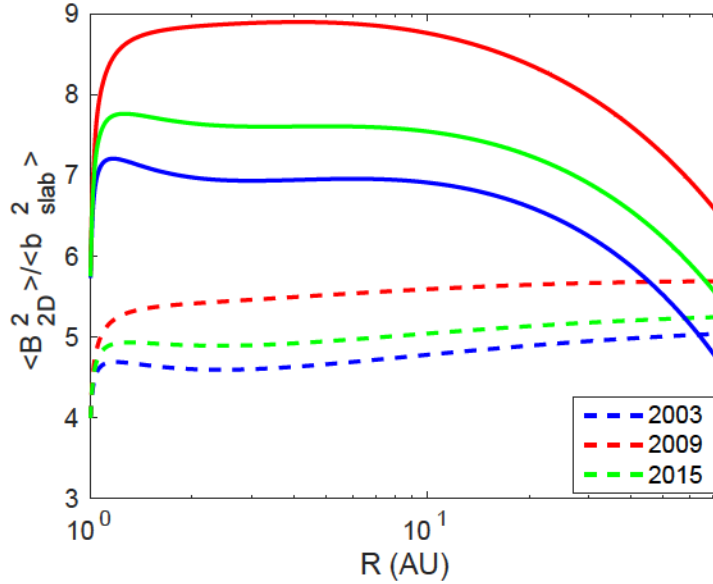


**Figure 1.** Evolution of the power anisotropy in magnetic field fluctuations as a function of heliocentric distance with no interplanetary source of turbulence. The solid curves correspond to the inertial range and the dashed curves to the energy-containing range.

characteristics for solar minimum and solar maximum. However, the  $\langle B_{2D}^2 \rangle / \langle b_{slab}^2 \rangle$  ratio for the inertial range decreases beyond 10 au.

Stream-shear and pickup ion sources of turbulence are always present, and drive solar wind turbulence throughout the heliosphere [39]. Furthermore, these sources of turbulence depend on heliospheric location in that the stream-shear source of turbulence is effective within  $\sim 5$  au, and the pickup ion source of turbulence beyond  $\sim 5$  au. Figure 2 shows the evolution of  $\langle B_{2D}^2 \rangle / \langle b_{slab}^2 \rangle$  with heliocentric distance when only stream-shear sources of 2D and slab turbulence are included in the NI turbulence transport model. Equations (9) and (10) are the stream-shear and pickup ion sources of 2D and slab turbulence. Zhao et al [37] calculated a form of stream-shear source of turbulence ( $\Delta UV_A^2$ ) observationally at 1 au from 1995 through 2017. Zhao et al [37] found that the stream-shear source of turbulence is stronger during solar maximum than solar minimum. The bottom row of Table 2 shows the values of  $\Delta UV_A^2$  for the years 2003, 2009, and 2015, which clearly makes the 2D and slab stream-shear sources of turbulence solar cycle dependent. In this case, the dashed blue, red, and green curves are very similar, unlike the dashed curves in Figure 1. Similarly, all the solid curves (blue, red, and green) are also almost identical. The results show that the anisotropy of magnetic field fluctuations in the inertial range is larger than in the energy-containing range. The anisotropy is  $\sim 5.5$  for the inertial range and slightly less than  $\sim 4$  for the energy-containing range throughout the heliosphere if only a shear-driving source is included.

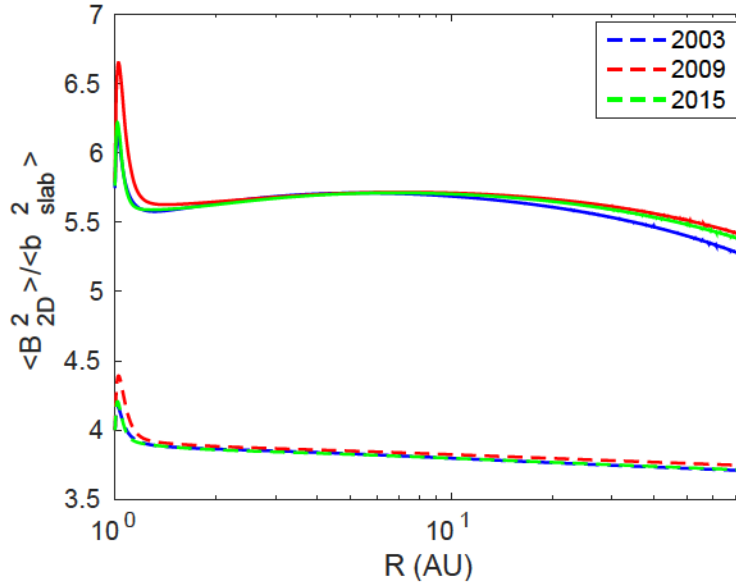


**Figure 2.** Evolution of the power anisotropy in magnetic field fluctuations as a function of heliocentric distance for a stream-shear source of turbulence. The solid and dashed curves are as in Figure 1.

When a pickup ion source of slab turbulence is also included in the NI turbulence transport model equations, the evolution of the anisotropy in magnetic field fluctuations in the energy-containing and inertial ranges with distance is shown in Figure 3. Equation (10) is a pickup ion source of slab turbulence for our turbulence transport model. The values of the solar wind speed, the solar wind density, and the Alfvén speed in Equation (10) for the years 2003, 2009, and 2015 are shown in Table 3. It makes a pickup ion source of turbulence solar cycle dependent, but a more detailed study is required in order to understand the dependence of pickup ion source of turbulence on solar cycle. We find that the  $\langle B_{2D}^2 \rangle / \langle b_{slab}^2 \rangle$  ratio for the energy-containing and inertial ranges decreases with the inclusion of a pickup ion source of turbulence. However, it is interesting to note that the solid and dashed red curves associated with solar minimum decrease at a smaller heliocentric distance than the solid and dashed blue and green curves associated with solar maximum. Figure 3 indicates that the ratio of the variances of the 2D and slab magnetic field fluctuations for both the energy-containing and inertial ranges beyond  $\sim 3$  au follow the ordering  $(\langle B_{2D}^2 \rangle / \langle b_{slab}^2 \rangle)_{2003} > (\langle B_{2D}^2 \rangle / \langle b_{slab}^2 \rangle)_{2015} > (\langle B_{2D}^2 \rangle / \langle b_{slab}^2 \rangle)_{2009}$ , and within  $\sim 3$  au the  $(\langle B_{2D}^2 \rangle / \langle b_{slab}^2 \rangle)_{2009}$  ratio is larger than the  $(\langle B_{2D}^2 \rangle / \langle b_{slab}^2 \rangle)_{2003}$  and  $(\langle B_{2D}^2 \rangle / \langle b_{slab}^2 \rangle)_{2015}$  ratios. It clearly shows that the ratio of the variances of 2D and slab magnetic field fluctuations associated with a solar minimum is different from the ratio of the variances associated with a solar maximum. Prior to the onset of pickup ion driving beyond  $\sim 5$  au, the energy-containing and inertial ranges anisotropies are the same as in Figure 2. With the dominance of pickup ion driving turbulence beyond 10 – 20 au, the anisotropies for both energy-containing and inertial ranges approach  $\sim 1$ .

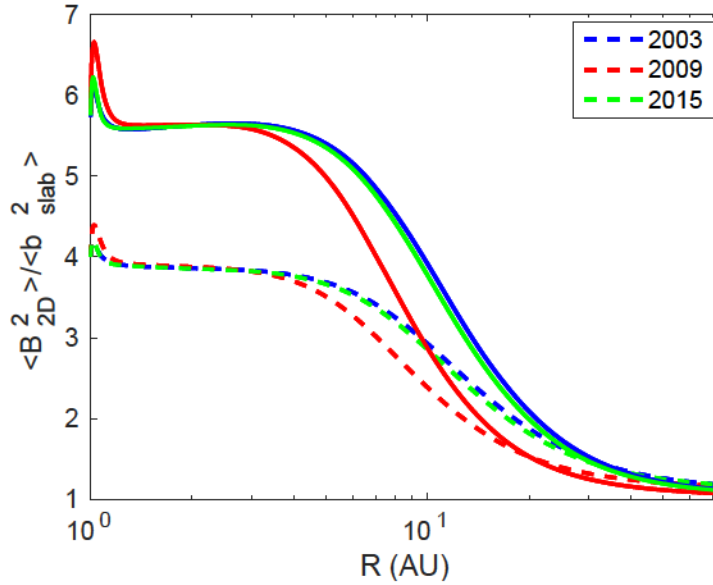


**Figure 3.** Evolution of the power anisotropy in magnetic field fluctuations as a function of heliocentric distance for both a stream-shear and pickup ion sources of turbulence. The solid and dashed curves are as in Figure 1.

#### 4. Discussion and Conclusions

In this paper, we investigated the evolution of anisotropy in magnetic field fluctuations at different levels of solar activity as a function of heliocentric distance. For this we used the Zank et al [31] NI turbulence transport model equations, the Adhikari et al [33] model for anisotropy of magnetic field fluctuations, and the boundary conditions from the Zhao et al [37] observational analysis. We calculated the ratio of the variances of the magnetic field fluctuations  $\langle B_{2D}^2 \rangle / \langle b_{slab}^2 \rangle$  for three cases; i) no source of turbulence, ii) stream-shear sources of 2D and slab turbulence, and iii) stream-shear sources of 2D and slab turbulence, and a pickup ion source of slab turbulence. We find that the ratios of the variances of the 2D and slab magnetic field fluctuations in the energy-containing and inertial ranges during the 2009 solar minimum are different from the ratios of the variances in the energy-containing and inertial ranges during the 2003 and 2015 solar maxima.

In the absence of a source of turbulence in the turbulence transport model, we find that the  $\langle B_{2D}^2 \rangle / \langle b_{slab}^2 \rangle$  ratio associated with the 2009 solar minimum in the energy-containing range increases monotonically with heliocentric distance, while  $\langle B_{2D}^2 \rangle / \langle b_{slab}^2 \rangle$  associated with the 2003 and 2015 solar maxima decreases slightly between  $\sim 1.2 - 2$  au, and then increases with heliocentric distance. The ratio of the variances during solar minimum is larger than the ratio of the variances during solar maximum. Furthermore, the  $\langle B_{2D}^2 \rangle / \langle b_{slab}^2 \rangle$  ratio in the inertial range during 2009 solar minimum is larger than the ratios of variances during the 2003 and 2015 solar maxima, in which the  $\langle B_{2D}^2 \rangle / \langle b_{slab}^2 \rangle$  ratio in the inertial range decreases beyond  $\sim 10$  au. The anisotropies for both

energy-containing and inertial ranges remain large throughout the heliosphere and the anisotropy in the inertial range is larger than the anisotropy in the energy-containing range. In this study, we assumed an 80:20 ratio between 2D and slab turbulence energies, and a 2:1 ratio between slab and 2D correlation lengths. Depending on the assumptions related to the turbulence energies and the correlation lengths, the evolution of anisotropies can be different as suggested by Verdini and Grappin et al [40], who find that the evolution of turbulent spectrum depends strongly on its initial anisotropy.

With the inclusion of 2D and slab stream-shear sources of turbulence in the NI turbulence transport model, we find that  $\langle B_{2D}^2 \rangle / \langle b_{slab}^2 \rangle$  in the energy-containing and inertial ranges is less than the  $\langle B_{2D}^2 \rangle / \langle b_{slab}^2 \rangle$  ratio when a source of turbulence is not included in the turbulence transport model. It indicates that a stream-shear source of turbulence reduces the anisotropy in magnetic field fluctuations. In this study, a stream-shear source of 2D turbulence is three times larger than a stream-shear source of slab turbulence, which is indicated by the chosen stream-shear driving constants shown in the Table 3. These anisotropies in magnetic field fluctuations results can be different for different 2D and slab stream-shear driving constants. Adhikari et al [33] calculated the anisotropy in magnetic field fluctuations in the energy-containing and inertial ranges for different stream-shear sources of slab turbulence with the same stream-shear source of 2D turbulence, and found that the anisotropy in magnetic field fluctuations decreases with an increase in the stream-shear source of slab turbulence. The  $\langle B_{2D}^2 \rangle / \langle b_{slab}^2 \rangle$  ratio in the energy-containing range during 2009 solar minimum is larger than the  $\langle B_{2D}^2 \rangle / \langle b_{slab}^2 \rangle$  ratio during the 2003 and 2015 solar maxima from 1 to 75 au. The  $\langle B_{2D}^2 \rangle / \langle b_{slab}^2 \rangle$  ratio in the inertial range for the 2009 solar minimum is larger than that of the 2003 and 2015 solar maxima from 1 to  $\sim 2$  au, after which the three ratios are approximately similar between  $\sim 2 - 10$  au. Eventually, the ratio during solar minimum becomes larger than the ratios during solar maxima beyond  $\sim 10$  au. We also find that the ratio of the variances in the inertial range is larger than the ratio of the variances in the energy-containing range. The energy-containing and inertial ranges anisotropies are  $\sim 5.5$  and  $\sim 4$ , respectively, throughout the heliosphere.

The inclusion of both 2D and slab stream-shear sources of turbulence and a pickup ion source of slab turbulence in the turbulence transport model yields ratios of  $\langle B_{2D}^2 \rangle / \langle b_{slab}^2 \rangle$  in the energy-containing range for solar maxima and minimum that are approximately similar from  $\sim 1.2$  to  $\sim 4$  au, after which the ratio corresponding to the 2009 solar minimum decreases beyond  $\sim 4$  au, while the ratios corresponding to the 2003 and 2015 solar maxima decrease beyond  $\sim 5$  au. The ratios of the 2D and slab magnetic field fluctuations in the energy-containing range from 1 au to  $\sim 4 - 5$  au is  $\sim 4$ , which eventually decreases to  $\sim 1$  at 75 au. The  $\langle B_{2D}^2 \rangle / \langle b_{slab}^2 \rangle$  ratio in the inertial range during 2009 solar minimum increases sharply initially, then decreases rapidly, followed by a slight increase from  $\sim 1.2$  to  $\sim 3$  au, after which there is a gradual decrease with distance. Similarly, the  $\langle B_{2D}^2 \rangle / \langle b_{slab}^2 \rangle$  ratio in the inertial range of the 2003 and 2015 solar maxima increases and decreases rapidly within  $\sim 1.2$  au, gradually increases until  $\sim 4$  au, and then decreases with increasing heliocentric distance. The  $\langle B_{2D}^2 \rangle / \langle b_{slab}^2 \rangle$  ratio in the inertial range for the solar minimum is larger than the  $\langle B_{2D}^2 \rangle / \langle b_{slab}^2 \rangle$  ratio for the solar maxima from 1 to  $\sim 2$  au, and then it reverses in the outer heliosphere beyond  $\sim 2$  au.

## Acknowledgments

We acknowledge the partial support of the NSF EPSCoR RII-Track-1 Cooperative Agreement OIA-1655280, NSF-DOE award 1707247, NASA grants NNX08AJ33G, Subaward 37102-2, NNX14AC08G, NNX14AJ53G, A99132BT, RR185-447/4944336 and NNX12AB30G. G.P.Z. acknowledges the support of the International Space Science Institute (ISSI), both through the award of the 2017 Johannes Geiss Fellowship and in the framework of an International Team Project 504 entitled “Current Sheets, Turbulence, Structures and Particle Acceleration in the Heliosphere”.

## References

- [1] Montgomery, D. & Turner, L. 1981, *Physics of Fluids*, 24, 825
- [2] Matthaeus, W. H., Goldstein, M. L., & Roberts, D. A. 1990, *J. Geophys. Res.*, 95, 20673
- [3] Narita, Y., Sahraoui, F., Goldstein, M. L., & Glassmeier, K.-H. 2010, *Journal of Geophysical Research (Space Physics)*, 115, A04101
- [4] Bieber, J. W., Wanner, W., & Matthaeus, W. H. 1996, *J. Geophys. Res.*, 101, 2511
- [5] Zank, G. P., Matthaeus, W. H., Bieber, J. W., & Moraal, H. 1998, *J. Geophys. Res.*, 103, 2085
- [6] Shalchi, A., Bieber, J. W., Matthaeus, W. H., & Schlickeiser, R. 2006, *ApJ*, 642, 230
- [7] Montgomery, D., & Turner, L. 1981, *PhFl*, 24, 825
- [8] Shebalin, J. V., Matthaeus, W. H., & Montgomery, D. 1983, *JPLPh*, 29, 525
- [9] Grappin, R. 1986, *PhFl*, 29, 2433
- [10] Grappin, R., Velli, M., & Mangeney, A. 1993, *PhRvL*, 70, 2190
- [11] Goldreich, P., & Sridhar, S. 1995, *ApJ*, 438, 763
- [12] Ghosh, S., Matthaeus, W. H., Roberts, D. A., & Goldstein, M. L. 1998, *JGR*, 103, 23705
- [13] Horbury, T. S., Forman, M., & Oughton, S. 2008, *PhRvL*, 101, 175005
- [14] Podesta, J. J. 2009, *ApJ*, 698, 986
- [15] Narita, Y., Glassmeier, K.-H., Sahraoui, F., & Goldstein, M. L. 2010a, *PhRvL*, 104, 171101
- [16] Wicks, R. T., Horbury, T. S., Chen, C. H. K., & Schekochihin, A. A. 2010, *MNRAS*, 407, L31
- [17] Bruno, R., & Telloni, D. 2015, *ApJL*, 811, L17
- [18] Zank, G. P., Adhikari, L., Hunana, P., et al. 2017, *ApJ*, 835, 147
- [19] Robinson, D. C., & Rusbridge, M. G. 1971, *PhFl*, 14, 2499
- [20] Zweben, S. J., Menyuk, C. R., & Taylor, R. J. 1979, *PhRvL*, 42, 1270
- [21] Belcher, J. W., & Davis, L., Jr. 1971, *JGR*, 76, 3534
- [22] Montgomery, D. 1982, *PhyS*, 1982, 83
- [23] Matthaeus, W. H., Goldstein, M. L., & Roberts, D. A. 1990, *JGR*, 95, 20673
- [24] Milano, L. J., Dasso, S., Matthaeus, W. H., & Smith, C. W. 2004, *PhRvL*, 93, 155005
- [25] Ruiz, M. E., Dasso, S., Matthaeus, W. H., Marsch, E., & Weygand, J. M. 2011, *JGRA*, 116, A10102
- [26] Matthaeus, W. H., Dasso, S., Weygand, J. M., et al. 2005, *PhRvL*, 95, 231101
- [27] Osman, K. T., & Horbury, T. S. 2007, *ApJL*, 654, L103
- [28] Dasso, S., Milano, L. J., Matthaeus, W. H., & Smith, C. W. 2005, *ApJ*, 635, L181
- [29] Smith, C. W. 2003, in *AIP Conf. Ser. 679, Solar Wind Ten*, ed. M. Velli et al. (Melville, NY: AIP), 413
- [30] Zank, G. P., & Matthaeus, W. H. 1992, *JGR*, 97, 17189
- [31] Zank, G. P., Adhikari, L., Hunana, P., et al. 2017, *ApJ*, 835, 147
- [32] Zank, G. P., Adhikari, L., Hunana, P., et al. 2017, *Journal of Physics Conference Series*, 900, 012023
- [33] Adhikari, L., Zank, G. P., Hunana, P., et al. 2017, *ApJ*, 841, 85
- [34] Adhikari, L., Zank, G. P., Hunana, P., et al. 2017, *Journal of Physics Conference Series*, 900, 012001
- [35] Hunana, P., & Zank, G. P. 2010, *ApJ*, 718, 148
- [36] Adhikari, L., Zank, G. P., Telloni, D., et al. 2017, *ApJ*, 851, 117
- [37] Zhao, L.-L., Adhikari, L., Zank, G. P., Hu, Q., & Feng, X. S. 2018, *ApJ*, 856, 94
- [38] Zank, G. P. 2014, in *Transport Processes in Space Physics and Astrophysics*, ed. G. P. Zank (Berlin: Springer)
- [39] Zank, G. P., Matthaeus, W. H., & Smith, C. W. 1996, *JGR*, 101, 17093

- [40] Verdini, A., & Grappin, R. 2016, *ApJ*, 831, 179